



SEISMIC DESIGN OF CONCRETE WALLED BUILDINGS

Joshua S. PUGH¹, Laura N. LOWES² and Dawn E. LEHMAN³

ABSTRACT

Review of earthquake damage to reinforced concrete (RC) walled buildings and damage sustained by slender RC walls subjected to cyclic lateral loading in the laboratory suggests these components commonly exhibit compression-controlled flexural failure. In the laboratory, compression-controlled failure of walls typically results in rapid strength loss; in the field, compression-controlled failure could be expected to result in undesirable building performance and unacceptable collapse risk. To investigate the earthquake performance of walled buildings, a numerical model was developed to enable accurate simulation of compression-controlled flexural failure. The earthquake performance of a series of idealized ACI Code-compliant walled buildings ranging in height from six to thirty stories was assessed. The results of this work indicate the potential for shear-controlled failure in walled buildings designed using ASCE 7 (2010) procedures. The results of numerical simulation were used to develop 1) capacity-design procedures for shear, 2) recommendations for flexural demands for use in design to ensure that inelastic flexural response is isolated to well-defined locations, and 3) strength-reduction factors to achieve desired collapse risk.

EARTHQUAKE RESPONSE OF SLENDER CONCRETE WALLS

A review of earthquake damage to concrete walled buildings and of damage to slender concrete walls subjected to cyclic lateral loading in the laboratory indicates the potential for compression-controlled flexural failure, characterized by crushing of concrete and buckling of longitudinal reinforcement in the compression regions of the wall. In the laboratory, concrete crushing and reinforcement buckling typically occurs simultaneously and is followed by rapid strength loss. Figure 1 shows compression damage, characterized by concrete crushing and buckling of longitudinal reinforcement, to walls in modern buildings with poorly (Figure 1a and 1b) and well confined (Figure 1c) boundary elements following the recent 2010 Chile and 2011 Christchurch earthquakes. A review of earthquake damage to walled buildings around the world suggests that the damage patterns shown in Figure 1 are not unique. Figure 2 by Birely (2012) shows the percentage of walled buildings exhibiting various damage modes as determined from review of post-earthquake reconnaissance reports; compression-damage is the most commonly observed damage mode. Finally, the data in Figure 3 show that the potential for compression-controlled failure is observed also in the laboratory, with almost 50% of wall specimens of varying configurations (planar, barbell, T-shaped, and C-shaped) tested in the laboratory under cyclic lateral loading exhibiting compression-controlled failure.

¹ EDG, Inc. Houston, TX, United States, josh.pugh@gmail.com

² Associate Professor, University of Washington, Seattle, WA, United States, lowes@uw.edu

³ Associate Professor, University of Washington, Seattle, WA, United States, delehman@uw.edu



a) Wall with compression damage, 17-story, mixed-use building constructed in 2009, Chile (Moehle 2012).



b) Wall with compression and shear damage, 12-story residential building constructed in 2006, Chile (Moehle 2012).



c) Wall with compression damage, 7-story commercial building, Christchurch, NZ (Kam et al. 2011).

Figure 1. Compression damage to modern concrete walled buildings following recent earthquakes.

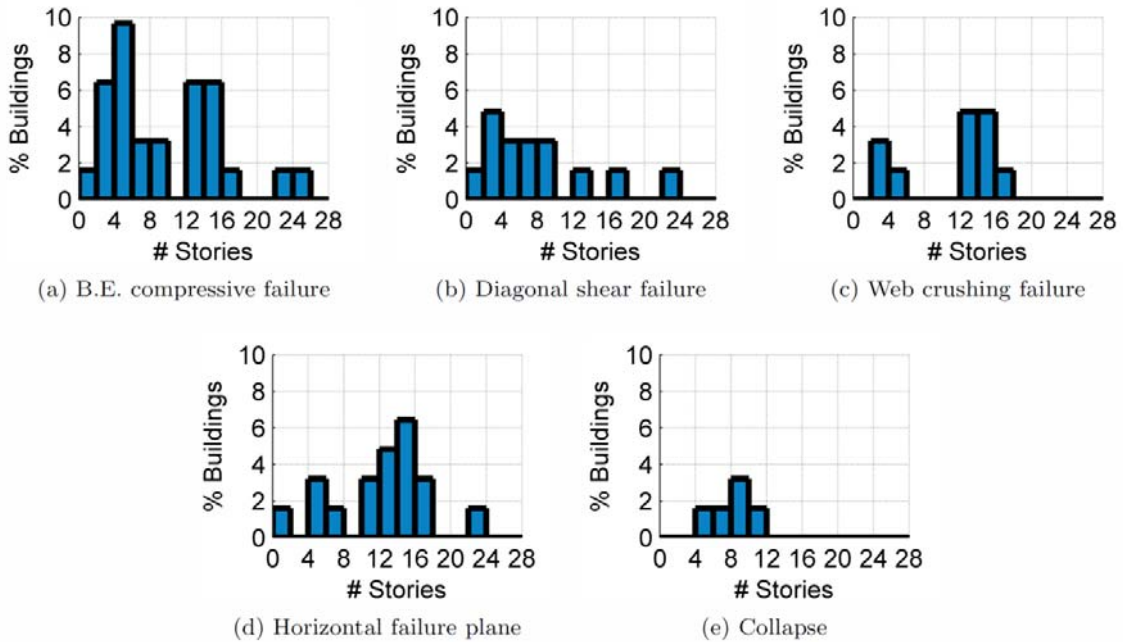


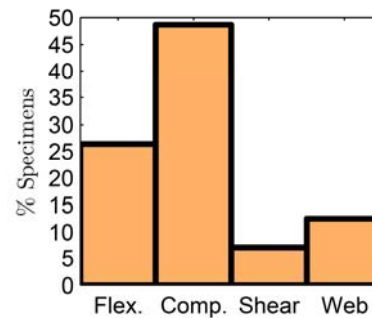
Figure 2. Damage observed in concrete walled buildings following major earthquakes since 1957 (Birely 2012).



a) Modern slender wall test specimen (PW4) at the end of laboratory testing; compression failure of right boundary element resulted in loss of lateral strength



b) Compression damage in boundary element of slender wall test specimen PW4 shown in a).



c) Percentage of wall test specimens exhibiting different failure modes in the laboratory.

Figure 3. Damage observed in slender concrete wall tests specimens in the laboratory (Birely 2012).

SIMULATION OF WALL RESPONSE

To investigate the earthquake performance of mid- to high-rise concrete walled buildings, accurate simulation of concrete walls, including accurate simulation of strength loss, is required. A wide range of models have been used to simulate the behavior of concrete walls exhibiting flexural response. These include multi-spring-element models, beam-column elements with lumped plasticity and distributed plasticity, and continuum models comprising shell elements and solid elements. Pugh (2012) reviewed nonlinear response models used currently in research and compared simulated and observed response histories for three commonly employed numerical models: the distributed-plasticity force-based and displacement-based fiber-type beam-column elements implemented in OpenSees (<http://opensees.berkeley.edu>) and the plane-stress RC continuum model implemented in VecTor2 (Wong and Vecchio 2006). Pugh concluded that i) no existing model provides accurate, mesh-objective, computationally efficient simulation of wall response through failure and ii) the distributed-plasticity force-based fiber-type beam-column element implemented in OpenSees provides the greatest opportunity for development to achieve accurate modeling (Pugh 2012).

To advance simulation of concrete walls, Pugh (2012) built on work by Coleman and Spacone (2001) addressing simulation of RC components using distributed-plasticity fiber-type beam-column elements. Coleman and Spacone demonstrate that for flexural RC components that exhibit softening due to concrete crushing, simulated drift capacity exhibits mesh sensitivity due to localization of deformation at the controlling section, and they propose regularization of the concrete constitutive model to achieve mesh-objective results. Regularization entails defining a unique concrete stress-strain curve for each fiber section in the beam-column element, with the post-peak portion of the concrete stress-strain curve defined by the integration length associated with the section and the concrete crushing energy, which is assumed to be a material property. Figure 4a shows a regularized concrete stress-strain model in which L_{IP} is the length associated with the section and G_{fc} is the concrete

crushing energy. Coleman and Spacone recommend values for the crushing energy of unconfined and confined concrete and demonstrate mesh-objective simulation of response for a reinforced column tested in the laboratory by Tanaka and Park (1990). Pugh (2012) demonstrates that achieving accurate, mesh-objective simulation of drift capacity for a set of 11 flexural walls exhibiting softening requires regularization of concrete and steel material models. Regularization of the stress-strain curve for reinforcing steel entails defining a unique steel stress-strain curve for each fiber section in the beam-column element, with the post-yield portion of the curve in tension and compression defined by the integration length associated with the section and the steel post-yield energy, which is assumed to be a function of the gage length used in material testing. Figure 4b shows the definition of the steel post-yield energy (G_{fs}) as a function of material test data (f_y , f_u , ϵ_y , $\epsilon_{u,exp}$) and the gage length used in material testing (L_{gage}); Figure 4c shows the regularized steel response model in which the regularized post-yield tangent stiffness ($b''E_s$) and regularized strain at ultimate strength (ϵ_u'') are functions of the steel post-yield energy (G_{fs}) and the integration length associated with the section (L_{IP}).

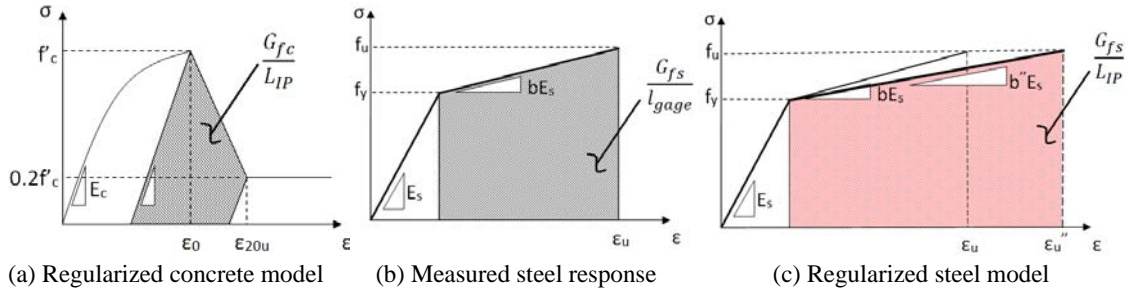


Figure 4. Stress-strain response histories employed in regularization of material response.

Using experimental data for 11 planar flexural wall test specimens that exhibited softening due concrete crushing and steel buckling under cyclic loading, Pugh (2012) developed recommendations for defining the crushing energy of unconfined concrete (G_{fc}) and confined concrete (G_{fcc}) as a function of concrete compressive strength:

$$G_{fc} = 2f'_c \text{ N/mm} \quad (1)$$

$$G_{fcc} = 1.70G_{fc} \quad (2)$$

where f'_c is the concrete compressive strength in MPa. These recommendations are appropriate for use with the force-based element formulation; the variation in axial load at the section level that is simulated using the displacement-based element formulation results in different crushing energy values being required for use with the displacement-based element. Unconfined concrete crushing energy (G_{fc}), was calibrated to provide, on average, accurate simulation of response for two planar walls constructed of unconfined concrete. Confined concrete crushing energy (G_{fcc}) was defined to provide, on average, accurate simulation of response for nine walls constructed of unconfined and confined concrete. Figure 5 shows the ratio of simulated to observed drift capacity as a function of the ratio of the confined to unconfined concrete crushing energy for the nine walls used to develop Eq. 2. The data in Figure 5 suggest that crushing energy is largest for walls with well-confined boundary elements and smallest for walls with poorly confined, rectangular boundary elements. The relationship between confinement and confined concrete crushing energy suggested by the data in Figure 5 was not included in Eq. 2 due to the small number of data points (Pugh 2012).

The regularized model was validated through comparison of simulated and observed response for a series of planar wall tests. Tests specimens were modeled using meshes comprising three force-based beam-column elements with three, five or seven integration points (i.e. fiber-type section models) along the length of the element. Three force-based elements were used because some specimens represented three-story subassemblages with loads applied at floor levels. Figure 6 shows a model with five integration points. A one-dimensional fiber-type discretization of the wall section was employed with an approximately constant fiber thickness of 1/32 of the depth of the confined boundary element; this level of mesh refinement was required to achieve accurate simulation of cyclic

response (Pugh 2012). Concrete material response was simulated using the OpenSees Concrete02 material model. Using this model, i) pre-peak response in compression is defined by the Hognestad model (1951), ii) post-peak response in compression is linear to a user-defined residual compressive strength, iii) tensile response is bilinear to a residual tensile strength of zero, iv) the unloading path from the compression envelope is bilinear and from the tension envelope is linear, v) reloading paths are linear, and vi) reloading in tension and compression occurs immediately upon unloading to a state of zero stress. Post-peak concrete response was defined using regularized material response parameters (Figure 4a); additional model parameters were defined as follows: i) for unconfined concrete, measured concrete compressive strength was used, ii) confined concrete strength was determined using the recommendations of Saatcioglu and Razi (1992), iii) given the Hognestad assumption of a parabolic pre-peak response curve, concrete strain at peak strength was defined such that the concrete modulus at zero strain was equal to that defined

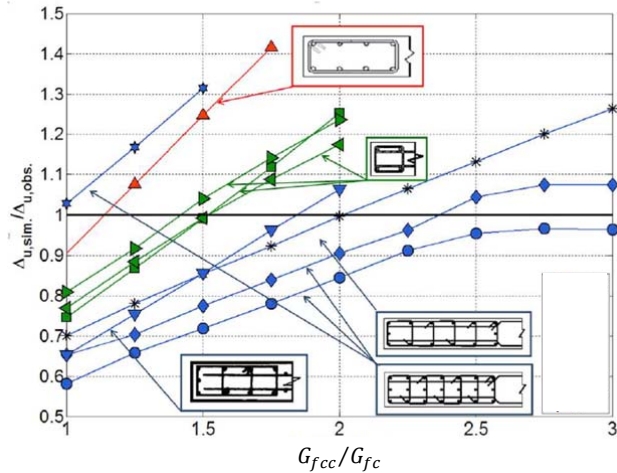


Figure 5. Ratio of simulated to observed drift capacity versus the ratio of confined to unconfined concrete crushing energy.

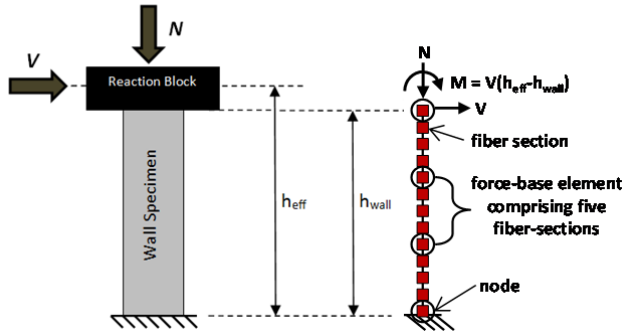


Figure 6. Planar wall test specimen subjected to lateral loading only at the top of the specimen and force-based element model.

by ACI 318 (2011), iv) residual compression strength was 20% of maximum strength, v) concrete tensile strength was defined equal a lower bound of $0.33\sqrt{f'_c}$ MPa ($4\sqrt{f'_c}$ psi) per Wong and Vecchio (2006) and vi) concrete post-peak stiffness in tension was defined equal to $0.05E_c$ per Yassin (1994). Steel material response was simulated using the OpenSees Steel02 model; this model employs a bilinear envelope with unload-reload paths defined using Mengetto-Pinto (1973) curves. Post-yield tangent stiffness was defined using regularized material response parameters; additional model parameters were defined using measured yield and ultimate strengths and measured strain at ultimate strength. The OpenSees MinMax material wrapper was used to simulate steel strength loss in tension at the regularized steel strain at ultimate strength (ϵ_u) and in compression at the regularized confined concrete strain at 80% strength loss (ϵ_{20u} in Figure 1a). Simulation of steel compression failure was intended to represent steel strength loss due to steel buckling at the compressive strain at which confinement from concrete was lost due to concrete compressive failure. Shear flexibility was included in the model, with elastic shear stiffness defined equal to 10% of the gross section stiffness per Lowes et al. (2009).

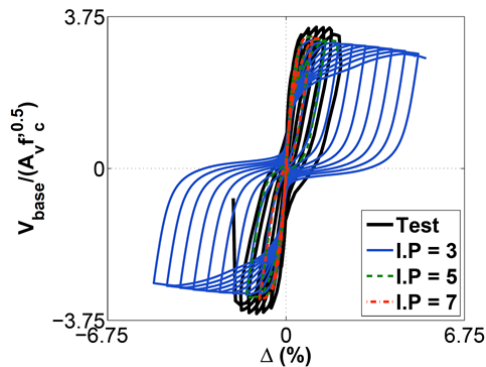
A data set comprising 18 planar wall test specimens was assembled for the model validation study; Pugh (2012) provides details for the test specimens. Specimens exhibited flexural response with failure resulting from simultaneous concrete crushing and steel buckling (CB), steel fracture following buckling (BR), or steel fracture prior to buckling (R). Table 1 presents statistics for the ratio of simulated to observed stiffness, strength and drift capacity for specimens grouped according to failure mode and for entire data set. Note that yield stiffness was defined using the displacement at the strength corresponding to simulated first yield of longitudinal reinforcement and that drift capacity was defined as the displacement at 20% strength loss. Figure 7 presents simulated and observed response histories for a typical specimen where response is simulated using the basic, unregularized

model (Figure 7a) and the regularized model (Figure 7b). Results of the validation study support the following conclusions:

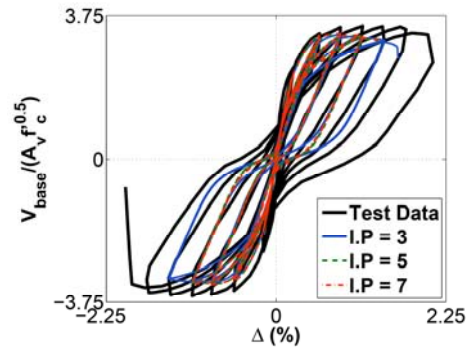
1. Peak base shear strength of all walls was accurately simulated by all force-based element meshes considered. The mean simulated to observed peak strength ratio was 0.94 with a coefficient of variation of 0.04 for compression controlled wall specimens and 0.99 with a coefficient of variation of 0.06 for tension controlled specimens.
2. Secant stiffness to yield was accurately simulated by all force-based element meshes considered. For all walls, the mean simulated to observed yield stiffness ratio was 1.02 with a coefficient of variation of 0.09.
3. Drift capacity data for walls failing due to flexural compression (CB) show a small dependency on the number of integration points. However, this is a vast improvement over the unregularized model which was found to have an average ratio of simulated to observed drift capacity ranging from 2.31 to 1.24 for models comprising a single force-based element with 3 and 7 integration points, respectively.
4. For the two (2) specimens failing due to tension rupture prior to significant buckling (R), drift capacity was slightly overestimated by the model, with a mean simulated to observed drift capacity ratio of 1.11 for the five fiber-section model.
5. For the five (5) specimens failing due to tension rupture after significant buckling (BR) and identified as softening systems, drift capacity was again slightly overestimated (ratios of simulated to observed drift capacity ranged from 1.06 to 1.11 for models with three, five and seven integration points), the coefficient of variation for these ratios was relatively high (ratios ranged from 0.29 to 0.22), and some mesh dependency was observed. The overestimation of and variation in simulated drift capacity likely results from the simplicity with which strength deterioration due to buckling of reinforcing steel was simulated; however, these results are likely acceptable for most applications.

Table 1: Ratio of simulated to observed response quantity for regularized wall model.

Failure Mode	No. of Tests		Yield Stiffness Ratio			Strength Ratio			Drift Capacity Ratio		
			3 IP	5 IP	7 IP	3 IP	5 IP	7 IP	3 IP	5 IP	7 IP
CB	11	Mean	1.01	1.02	1.02	0.95	0.94	0.94	0.96	0.97	1.02
		COV	0.09	0.09	0.10	0.04	0.04	0.04	0.14	0.14	0.17
BR	5	Mean	1.01	1.01	1.01	0.96	0.95	0.95	1.06	1.08	1.11
		COV	0.11	0.11	0.11	0.06	0.05	0.05	0.29	0.22	0.23
R	2	Mean	1.05	1.04	1.04	0.99	1.00	0.99	1.04	1.11	1.18
All	19	Mean	1.02	1.02	1.02	0.96	0.95	0.95	1.00	1.02	1.06
		COV	0.09	0.09	0.09	0.05	0.04	0.04	0.19	0.17	0.19



(a) Standard, unregularized material models



(b) Regularized material models

Figure 7. Simulated and measured normalized base shear versus drift response for planar wall WSH6 tested by Dazio et al. (2009). Note that base shear is presented in US customary units.

PERFORMANCE OF US CODE-COMPLIANT CONCRETE WALLED BUILDINGS

To improve understanding of the earthquake performance of US code-compliant concrete walled buildings, idealized buildings were designed and assessed using the regularized beam-column model presented above and the FEMA P695 (2009) methodology. Four core-wall buildings with a 100 ft. by 100 ft. footprint and ranging in height from 16 to 20 stories were designed using current codes and standard practice. For each building height, designs were completed for demands determined using the ASCE 7 equivalent lateral force (ELF) procedure and using the results of model response spectrum analysis (MRSA); MRSA demands were scaled such that the base shear demand was equal to that determined using the ELF procedure. Details of the design process included the following: i) the core-wall system was assumed to be located at the center of the building and comprise two coupled c-shape walls, ii) assumed seismic weight of 170 psf, gravity weight of 190 psi and wall axial load at the base of $0.1f_cA_g$, iii) earthquake base shear demands determined per ASCE 7 (2010) for seismic design category D with $R = 6$ and $C_d = 5$, iv) walls were sized for shear per *Seismic Design of Cast-in-Place Concrete Special Structural Walls and Coupling Beams* (NIST 2011), v) wall longitudinal reinforcement layout was uniformly distributed over the cross section of the wall, designed to meet strength requirements at the base of the wall, and continued up the entire height of the wall, and vi) wall capacities and detailing were determined using ACI 318-11. OpenSees models of the idealized walled buildings were created that included i) regularized beam-column elements with elastic shear stiffness used to model the wall, ii) seismic mass uniformly distributed to wall nodes, iii) gravity load uniformly distributed over the height of the building, with a portion of the load applied to wall nodes to generate the desired axial load at the base of the wall, iv) the remaining gravity load was uniformly distributed over the height of the building and applied to a p-delta column that contributed no lateral stiffness, and v) 2% Rayleigh damping was assumed. Incremental time-history analyses (ITHAs) were performed for each of the ground motion records included in the P695 far-field ground motion set, with ground motions scaled on the basis of the spectral acceleration at the design period of the building (T_1), which was the ASCE 7 upper limit of C_uT_a . Earthquake ground motion was assumed to act only in the direction of wall webs; response in the direction perpendicular to the web of the walls, which would induce coupling of the walls due to the presence of coupling beams, was not considered.

The analysis results indicate that all building designs could be expected to exhibit shear failure at earthquake intensities far below the design basis event (DBE). Specifically, the data show that median maximum shear demand exceeded the probable shear capacity (determined per ACI 318 using expected material strengths rather than design strengths) for earthquake intensities exceeding approximately 30% of the maximum considered earthquake (MCE). Note that the intensity of the DBE is 67% of the MCE. Figure 8 shows, for the 20-story building, the ratio of the median of the maximum simulated shear demands (V_{ITHA}) computed for each of the ground motions included in the P695 far-field ground-motion suite to the shear capacity computed using expected rather than design material strengths ($V_{n,pr}$) versus the median earthquake intensity of the ground motion suite relative to the intensity of the MCE. Data for other building heights were similar to those in Figure 8.

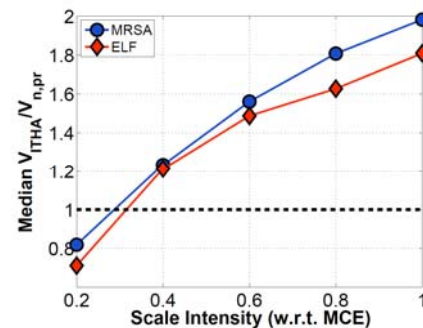


Figure 8. Ratio of median shear demand to expected shear capacity versus earthquake intensity relative to the MCE

SEISMIC DESIGN OF SLENDER WALLS: SHEAR DEMAND

To reduce the likelihood of shear failure in slender walls, a new capacity-design approach for shear was developed. Development of the new approach started with an evaluation of shear demand in slender wall buildings and an evaluation of existing capacity-design procedures for shear. To accomplish these evaluations, a second set of concrete walled buildings was designed. Sixty-four (64) idealized walled buildings ranging in height from 6 to 24 stories were designed using the design process outlined above, with the following exceptions: i) planar walls were employed for building

heights of 12 stories or less and c-shaped walls were employed for building heights greater than 12 stories ii) for each building height, walls were sized to achieve fundamental periods ranging from $0.08N$ to $0.20N$, where N is the number of building stories and the period range is approximately equal to the ASCE 7 empirical upper limit on the design period, $C_u T_a$, and iii) for each building height and period, strength reduction factors of 2, 3 and 4 were used to design longitudinal reinforcement; these strength reduction factors were applied directly to demands determined from MRSA and were not scaled to meet demands determined from the ELF procedure. Nonlinear ITHA were conducted for all of the walled building designs using a suite of seven synthetic ground motions. The synthetic motions were constructed to provide a best fit to the ASCE 7 design spectrum and employed to reduce variability in simulated response resulting from earthquake ground motion variability. Motions were applied only in one direction; parallel to planar walls and the web of the c-shaped walls.

For this second set of walled building designs, nonlinear analysis results were consistent with previous results. Maximum shear demand determined from nonlinear analysis significantly exceeded design shear demand determined from MRSA. Previous research (Blakeley et al. 1975) demonstrates that for walls exhibiting nonlinear response, amplification of shear demand, over that predicted from elastic analysis, results from flexural over-strength and from dynamic amplification. The actual flexural capacity of a wall exceeds the design demand due to code-based strength requirements and actual material strengths that exceed design strengths. Since flexural yielding is the expected response mechanism for concrete walls, actual shear demand is necessarily a function of flexural capacity. Thus, flexural over strength results in actual shear demands that exceed design demands. While flexural yielding at the base of the wall limits shear demand due to first-mode seismic demands (first-mode seismic demands produce a maximum moment at the base of the wall), flexural yielding at the base of the wall does not limit higher-mode seismic demands. Ultimately, this results in a drop in the effective height at which the resultant seismic shear acts and an increase, over that predicted using elastic analysis, in the base shear associated with the wall achieving flexural strength at the base. This increase in shear demand associated with dynamic response of the yielding wall is typically identified as dynamic amplification.

A capacity-design procedure for shear requires accurate prediction of shear demand for the range of wall heights and configurations found in practice. Flexural over-strength is relatively constant with building height and period, and the impact of flexural over-strength on shear demand is easily estimated. Pugh (2012) recommends that an over-strength factor of 1.4 to 1.5 be used; this is consistent with NIST (2011) and Priestley et al. (2007). However, prediction of dynamic amplification is more challenging. Figure 9 shows the ratio of the dynamic amplification factor computed using previously proposed methods, ω_v , to the dynamic amplification factor computed from nonlinear analysis results, with $\omega_{ITHA} = V_{ITHA}/V_u/\Omega_o$, where V_{ITHA} is the maximum shear demand computed for the ITHA of the walled building, V_u is the design shear demand and Ω_o is the computed flexural over-strength, with $\Omega_o = M_{pr}/M_u$, where M_{pr} is the flexural capacity of the wall computed using probably material properties and M_u is moment demand used for design. The data in Figure 9 show i) the method proposed by Eibl provides the best prediction of dynamic amplification, ii) the Eibl method is precise but slightly unconservative for shorter buildings and relatively imprecise for taller buildings, iii) the NZ 3101 and SEAOC methods are unconservative for buildings of all heights designed using strength reduction factors greater than 3, and iv) The Priestley et al. method is relatively accurate and precise for shorter buildings but overly conservative for taller buildings. On the basis of the data in Figure 9 it was concluded that additional research to develop an improved method for determining a dynamic amplification factor for shear was warranted.

To improve prediction of shear demand and thereby enable capacity design for shear, the Eibl method was modified. Using the Eibl method, shear demand is computed as the sum of the reduced first-mode shear and unreduced higher mode shear demands. This approach follows from the assumptions that i) first-mode response dominates system response, ii) inelastic action is limited to the first-mode with higher-modes responding essentially elastically, and iii) shear demand may be computed as the sum of the reduced first-mode shear and the unreduced higher-mode contributions to base shear. However, evaluation of the ITHA data shows that as building height increases, higher mode contributions to base shear begin to dominate over first mode contributions. This is assumed to produce the observed inaccuracy in predicted dynamic amplification for taller buildings that is shown in Figure 9c. Thus a modified MRSA method was developed in which the mode that represents the

largest contribution to the base shear is identified (typically the first or second mode) and the design shear is defined equal to sum of the reduced shear forces associated with this mode and the unreduced forces associated with all other modes.

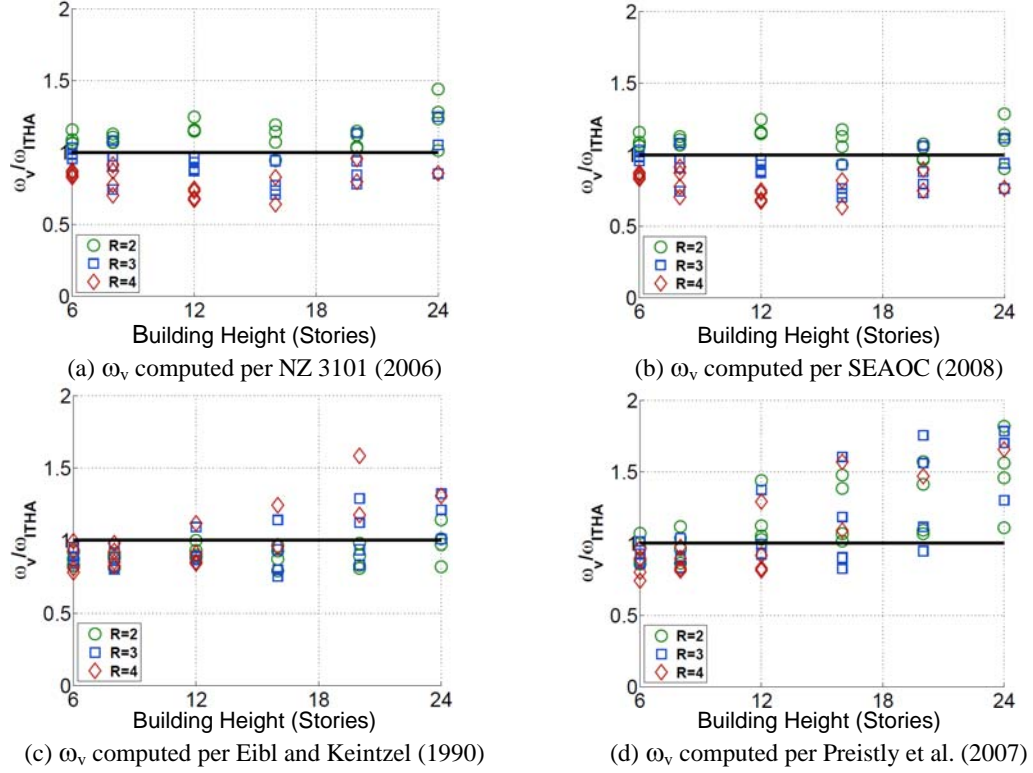


Figure 9. Ratio of predicted to simulated dynamic amplification for walled buildings of varying heights.

Figure 10 shows the ratio of dynamic amplification computed using the proposed approach, ω_v , to dynamic computed as described previously from nonlinear analysis results, ω_{TTHA} . The data in Figure 10 show that using the proposed approach, dynamic amplification of shear can be computed precisely, though slightly unconservatively, for the full range of building heights typically considered in design. The slight unconservatism is attributed to the fact that design shear demand is determined assuming 2% damping in all modes while shear demand from nonlinear analysis employs Rayleigh damping of 2% for periods of $1.5T_1$ and T_2 , with substantially smaller damping ratios achieved for periods between $1.5T_1$ and T_2 . To achieve accurate and precise prediction of shear demand, shear demand computed as above can be increased by 10%.

Thus, a capacity-design procedure for shear in slender concrete walls is proposed in which

$$\phi V_n \geq \Omega_o \beta V_u \quad (3)$$

where ϕ is the code-based strength reduction factor for shear, V_n is the code-based shear strength, $\Omega_o = 1.4$ to account for increased shear demand due to flexural over-strength, $\beta = 1.1$ to account for assumption of increased damping in elastic analysis, and V_u is the shear demand computed using the results of linear elastic MRSA with a code-based strength reduction factor applied only to the one mode that represents the largest contribution to the base shear and demands from all other modes remaining unreduced.

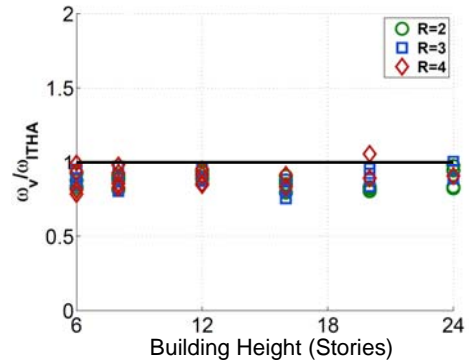


Figure 10. Ratio of predicted to simulated dynamic amplification factor.

SEISMIC DESIGN OF SLENDER WALLS: FLEXURAL DEMAND

With the above capacity-design procedure for shear limiting the risk of shear failure, the research effort focused on the expected earthquake performance of walls designed per US codes and standard practice and exhibiting flexure-controlled response. To improve understanding of the earthquake performance of walls responding in flexure, a series of nine walled buildings ranging in height from 6 to 24 stories was designed using the capacity-design procedure for shear presented above, the design process described above and US standard practice with the exception that four different approaches for defining the shape of the moment demand envelope employed for design of longitudinal reinforcement up the height of the wall were considered. These approaches included i) employing the demand enveloped determined from the MRSA analysis such that longitudinal reinforcement was reduced at intervals up the height of the wall until the ACI Code minimum reinforcement ratio was reached, ii) following the recommendations of Paulay and Priestley (1992) and SEAOC (2006) in which the moment demand at the base is assumed to extend up to a height equal to the horizontal length of the wall and then diminish linearly to zero at the top of the wall, and iii) employing a variation of the dual-hinge design method recommended by Panagioutou and Restrepo (2009) in which the cross-section at the base of the wall was maintained over the entire height of the wall except for a region just above mid-height where the flexural strength of the wall was significantly weakened. In all cases, walls were designed such that the factored flexural strength of the wall exceeded the reduced flexural demands, where the flexural demand defining the demand envelope was determined using the results of MRSA with a strength reduction factor of 3 was applied directly to the MRSA demand.

The earthquake performance of the idealized buildings was assessed on the basis of results of nonlinear dynamic analyses performed using the numerical modeling approach and the suite of seven synthetic ground motion records scaled to the DBE and MCE. Figure 11 shows median curvature demand, defined as the maximum curvature demand divided by the yield curvature, for the 6-story building, the three demand envelopes and the MCE. These data show that when demands are determined i) directly from MRSA results, inelastic flexural response occurs over the entire height of the walls with large ductility demands at the base of the wall, ii) using the Paulay and Priestley envelope, inelastic action is limited to the base of the wall, iii) using the Panagioutou and Restrepo dual hinge method inelastic action is limited to the base of the wall and the designer-specified second-hinge location, though it should be noted that inclusion of the second hinge does not diminish ductility demands at the base of the wall. Similar results were observed for the 6- and 20-story designs. For the Paulay and Priestley and Rangiotou and Restrepo demand envelopes, inelastic action is limited to those regions where it is expected to occur. This is not the case for the MRSA-based demand envelope. Copious volumes of transverse reinforcement are required to ensure ductile response in regions where significant inelastic action is expected. Thus, if the MRSA-based demand envelope is used, copious volumes of transverse reinforcement are required over a large portion of the wall. Given this, the results of this study suggest that the Paulay and Priestley and Pagioutou and Restrepo envelopes are preferred to the MRSA-based approach.

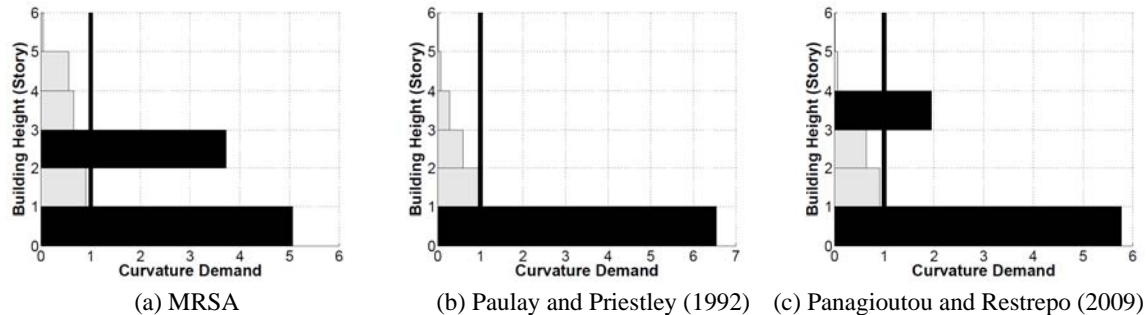


Figure 11. Median curvature demand for different flexural demand envelopes for 6-story walled building subjected to suite of seven synthetic motions scaled to the MCE

SEISMIC DESIGN OF SLENDER WALLS: STRENGTH REDUCTION FACTORS

The above recommendations for determining design demands will improve the earthquake performance of concrete walled buildings over that expected for buildings designed using current US design codes and standard practice. Further research was required to determine strength reduction factors for use in design to ensure that walled buildings exhibit the desired earthquake collapse risk. A series of nine buildings ranging in height from 6 to 20 stories was designed using i) either the shear-capacity procedure described above or shear demand determined directly from elastic analysis as is current standard practice in the US, ii) flexural demand envelope by Priestley and Paulay (1992) or Panagioutou and Restrepo (2009), and iii) demands determined by applying a strength reduction factor of $R = 3$ directly to MRSA demands or using the ASCE 7 procedure in which a strength reduction factor of $R = 6$ is applied to MRSA demands and then demands are scaled to 100% of the EFL demand (this is approximately equivalent to $R = 4$ applied directly to MRSA demands). These buildings were then evaluated using the FEMA P695 methodology and results were used to estimate the R-factors required to achieve a collapse risk of 20% under the MCE.

The FEMA P695 methodology was developed to provide a rational basis for establishing and evaluating the seismic performance factors (i.e. R , C_d and Ω_o) used in ASCE 7. The methodology entails i) designing a series of buildings that comply with a set of design criteria and span the practical design space, and ii) performing nonlinear ITHA of the buildings, using a provided suite of earthquake ground motions, to assess collapse capacity. Collapse capacity is quantified in terms of a collapse margin ratio (CMR) that is the ratio between the ground motion intensity that causes collapse for more than half of the ground motions and the MCE intensity. Collapse risk is determined by computing an adjusted CMR (ACMR); the CMR is adjusted to account for spectral shape variations expected for extreme seismic events and for uncertainties in design, simulation and building idealization. While the preferred application of the P695 methodology is to demonstrate that a given set of seismic performance factors produces the desired collapse risk; however, the R-factor required to achieve a specific collapse risk may be estimated by assuming a linear relationship between R and ACMR in the vicinity of the desired R-factor.

Nonlinear ITHA of the 12 building designs were conducted and the P695 methodology was employed to estimate R-factors required to achieve a 20% collapse risk for the MCE. For 6- and 12-story buildings that employed planar walls, R-factors ranging from 2.5 to 2.7 were required to achieve the specified collapse risk. For the 20-story buildings that employed c-shaped walls, an R-factor of 3.9 or 3.6 was required to achieve the specified collapse risk. This increased R-factor is attributed to the wall flanges providing a wider compression zone that results in reduced compressive strain demands and, thus, delayed onset of compression-controlled flexural failure. On the basis of these results, R-factors of 2.5 and 3.5 are recommended for design of planar and c-shaped core walls, respectively.

CONCLUSIONS

Review of earthquake damage to concrete walled buildings and damage sustained by slender concrete walls in the laboratory suggests walls commonly exhibit compression-controlled flexural failure. Evaluation of existing response models for slender concrete walls shows that these models are not accurate, and that in particular these models do not provide accurate simulation of strength loss. A new response model for slender walls was developed using the force-based distributed-plasticity fiber-type beam-column element available in OpenSees. To provide accurate, mesh-objective prediction of strength loss, the model employs regularization of concrete and steel material response histories using concrete crushing energy, steel yield energy and mesh-dependent lengths. Crushing energies for confined and unconfined concrete were calibrated using data from laboratory tests of walls exhibiting compression-controlled failure. The model was applied to investigate the seismic performance of walled buildings and advance seismic design procedures. The results of nonlinear ITHA show that i) walls designed using current standard practice in the US could be expected to exhibit shear failure under moderate earthquake loading, ii) a newly developed capacity-design procedure for shear can significantly reduce the likelihood of shear failure, iii) use of the flexural demand envelopes proposed by Paulay and Priestly (1992) and Panagioutou and Restrepo (2009) can ensure that flexural yielding

is isolated to expected regions of the wall, and iv) strength reduction factors of 2.5 and 3.5, applied directly to demands determined from MRSA, are required to achieved desired collapse risk for planar and c-shaped walls, respectively.

REFERENCES

- ACI (2011). *Building Code Requirements for Structural Concrete (ACI 318-11) and Commentary (ACI 318R-11)*. American Concrete Institute, Committee 318, Farmington Hills, MI, 2008.
- ASCE (2010). *Minimum Design Loads for Buildings and Other Structures, ASCE/SEI 7-10*. Reston, VA.
- Birely AC (2012). Seismic performance of slender reinforced concrete structural walls. *PhD Dissertation*, University of Washington, 983 pp.
- Blakeley R, Cooney R, Megget L (1975). Seismic shear loading at flexural capacity in cantilever wall structures. *Bulletin of the New Zealand Society for Earthquake Engineering* 8(4): 278–290.
- Coleman J and Spacone E (2001). Localization issued in force-based frame elements. *ASCE Journal of Structural Engineering* 127(11): 1257–1265.
- Dazio A, Beyer K, Bachmann H (2009). Quasi-static cyclic tests and plastic hinge analysis of rc structural walls. *Engineering Structures* 31(7): 1556–1571.
- Eibl, Keintzel E (1990). Seismic design shear forces in RC cantilever shear wall structures. *European Earthquake Engineering* 3: 7–16.
- FEMA (2009). *Quantification of building seismic performance factors*. Federal Emergency Management Agency, Washington, D.C., Tech. Rep. No. FEMA P-695.
- Hognestad E (1951). *A Study of Combined Bending and Axial Load in Reinforced Concrete Members*, Bulletin 399, University of Illinois Engineering Experiment Station, Urbana, Ill., 128 pp.
- Kam WY, Pampanin S, Elwood K (2011). “Seismic Performance of Reinforced Concrete Buildings in the 22 February Christchurch (Lyttelton) Earthquake” *Bulletin of the New Zealand Society for Earthquake Engineering* 44(4): 239-278.
- Lowes LN, Oyen P, Lehman DE (2009). Evaluation and Calibration of Load-Deformation Models for Concrete Walls. *ACI-SP 265: Thomas T.C. Hsu Symposium: Shear and Torsion in Concrete Structures*. Ed. A. Belarbi, Y.L. Mo, A. Ayoub. Farmington Hills: American Concrete Institute: 171-198.
- Lowes, LN, Lehman DE, Birely AC, Kuchma DA, Marley KP, Hart CR (2012). “Earthquake Response of Slender Concrete Planar Concrete Walls with Modern Detailing” *Engineering Structures* 34: 455-465.
- Lehman DE, Turgeon J., Birely AC, Hart CR, Kuchma DA, Lowes LN, Marley KP (2014). Seismic Behavior of a Modern Concrete Coupled Wall. *Journal of Structural Engineering, ASCE* (139): 1371-1381.
- Menegotto M, Pinto P (1973). Method of Analysis for Cyclically Loaded Reinforced Concrete Plane Frames Including Changes in Geometry and Non-elastic Behavior of Elements under Combined Normal Force and Bending. *IABSE Symposium on Resistance and Ultimate Deformability of Structures Acted on by Well-Defined Repeated Loads, Final Report*.
- Moehle J (2012). Personal communication.
- NIST (2011). *Seismic design of cast-in-place concrete special structural walls and coupling beams* NEHRP Consultants Joint Venture for the National Institute of Standards and Technology, Gaithersburg, MD, Tech. Rep. No. GCR 11-917-11.
- NZS (2006). *Concrete Structures Standard, Part 1: The Design of Concrete Structures: Part 2: Commentary on the Design of Concrete Structures* S. N. Zealand, Wellington, New Zealand: NZS 3101.
- Panagiotou M, Restrepo J (2009). Dual-plastic hinge design concept for reducing higher-mode effects on high-rise cantilever wall buildings. *Earthquake Engineering & Structural Dynamics* 38(12).
- Paulay T, Priestley M (1992). *Seismic Design of Reinforced Concrete and Masonry Buildings*.
- Priestley M, Calvi G, Kowalsky M (2007). *Displacement-Based Seismic Design of Structures* I. Press, Italy.
- Pugh JS (2012). Numerical Simulation of Walls and Seismic Design Recommendations for Walled Buildings. *PhD Dissertation*, University of Washington, 448 pp.
- Saatcioglu M, Razvi S (1992). Strength and ductility of confined concrete. *ASCE Journal of Structural Engineering* 81(6): 1590–1607.
- SEAOC (2008). *Reinforced concrete structures*,” Structural Engineers Association of California, Sacramento, CA, Tech. Rep. Article 9.01.010.
- Tanaka H, Park R (1990). *Effect of lateral confining reinforcement on the ductile behavior of reinforced concrete columns*. Department of Civil Engineering, University of Canterbury, Christchurch, New Zealand, Tech. Rep. Report No. 90-2, 1990.
- Wong and Vecchio, *VecTor2 and FormWorks Users Manual*. University of Toronto, 2006.
- Yassin, M. (1994). Nonlinear analysis of prestressed concrete structures under monotonic and cyclic loads. *Ph.D. Dissertation*. University of California, Berkeley.